RESEARCH ARTICLE

The effect of stochastically perturbed parametrisation tendencies (SPPT) on rapidly ascending air streams

Moritz Pickl[1] | **Simon T. K. Lang[2]** | **Martin Leutbecher[2]** | **Christian M. Grams[1]**

[1]Institute of Meteorology and Climate Research (IMK–TRO), Department Troposphere Research, Karlsruhe Institute of Technology (KIT), Karlsruhe, Germany

[2]European Centre for Medium-Range Weather Forecasts (ECMWF), Reading, UK

Correspondence
M. Pickl, Karlsruher Institut für Technologie (KIT), Institut für Meteorologie und Klimaforschung, Postfach 3640, Karlsruhe 76021, Germany.
Email: moritz.pickl@kit.edu

Abstract

The stochastically perturbed parametrisation tendency (SPPT) scheme is a well-established technique in ensemble forecasting to address model uncertainty by introducing perturbations into the tendencies provided by the physics parametrisations. The magnitude of the perturbations scales with the local net parametrisation tendency, resulting in large perturbations where diabatic processes are active. Rapidly ascending air streams, such as warm conveyor belts (WCBs) and organized tropical convection, are often driven by cloud diabatic processes and are therefore prone to such perturbations. This study investigates the effects of SPPT and initial condition perturbations on rapidly ascending air streams by computing trajectories in sensitivity experiments with the European Centre for Medium-Range Weather Forecasts (ECMWF) ensemble prediction system, which are set up to disentangle the effects of initial conditions and physics perturbations. The results demonstrate that SPPT systematically increases the frequency of rapidly ascending air streams. The effect is observed globally, but is enhanced in regions where the latent heating along the trajectories is larger. Despite the frequency changes, there are only minor modifications to the physical properties of the trajectories due to SPPT. In contrast to SPPT, initial condition perturbations do not affect WCBs and tropical convection systematically. An Eulerian perspective on vertical velocities reveals that SPPT increases the frequency of strong upward motions compared with experiments with unperturbed model physics. Consistent with the altered vertical motions, precipitation rates are also affected by the model physics perturbations. The unperturbed control member shows the same characteristics as the experiments without SPPT regarding rapidly ascending air streams. We make use of this to corroborate the findings from the sensitivity experiments by analyzing the differences between perturbed and unperturbed members in operational ensemble forecasts of ECMWF. Finally, we give an explanation of how symmetric,

zero-mean perturbations can lead to a unidirectional response when applied in a nonlinear system.

1 | INTRODUCTION

Numerical weather prediction is intrinsically affected by uncertainties due to the nonlinear propagation of forecast errors in the chaotic atmosphere (Lorenz, 1963). The uncertainties arise from erroneous estimations of the initial conditions and from deficiencies in the formulation of the dynamics and physics in the model. The aim of ensemble forecasting is to represent these sources of uncertainty by running several integrations from slightly perturbed initial conditions and/or with a perturbed forecast model (e.g., Leutbecher and Palmer, 2008). A well-established technique to represent model uncertainty related to physical processes is the stochastically perturbed parametrisation tendency (SPPT) scheme, which has been used operationally at the European Centre for Medium-Range Weather Forecasts (ECMWF) since 1999 (Buizza *et al.*, 1999). Its main purpose is to increase ensemble spread by introducing state-dependent perturbations into the tendencies provided by the model physics. The perturbations are generated with a two-dimensional (2D) random field, which evolves in time and has prescribed variance as well as spatial and temporal correlations (Leutbecher *et al.*, 2017; Lock *et al.*, 2019). The assumption behind SPPT is that the error of the parametrisations is proportional to the net physics tendency (Buizza *et al.*, 1999). The random perturbation factor is drawn from a Gaussian distribution centred on the unperturbed tendency, resulting in symmetric perturbations over the forecast integration (Leutbecher *et al.*, 2017). SPPT increases the ensemble spread, which improves the reliability of the ensemble forecasts. It also has a positive impact on the probabilistic skill (Lang *et al.*, 2021) and can reduce systematic biases of the ensemble prediction system (Berner *et al.*, 2015; Leutbecher *et al.*, 2017; Wang *et al.*, 2019). For example, SPPT alters the frequency distribution of tropical precipitation rates and thereby reduces systematic biases (Subramanian *et al.*, 2017). Further, SPPT improves the representation of tropical convection in seasonal forecasts (Weisheimer *et al.*, 2014) and has a positive impact on the tropical cyclone activity in seasonal forecasts (Stockdale *et al.*, 2018) and climate simulations (Vidale *et al.*, 2021). Moreover, SPPT is capable of triggering noise-induced regime transitions (Berner *et al.*, 2017). Christensen *et al.* (2015)

and Dawson and Palmer (2015) report improved weather regime behaviour in the Euro-Atlantic sector in idealized and comprehensive model simulations with SPPT compared with deterministic parametrisation schemes, and Davini *et al.* (2021) report effects of SPPT on atmospheric blocks.

In this study, we look at the impact of SPPT from a process-oriented weather system perspective by analyzing the effects of SPPT on rapidly ascending air streams, which in the Extratropics are predominantly related to the warm conveyor belt (WCB). WCBs are moist air streams in the vicinity of extratropical cyclones, which ascend cross-isentropically from the planetary boundary layer into the upper troposphere, typically within about 1–2 days (Carlson, 1980; Wernli and Davies, 1997). When reaching the tropopause level, the divergent outflow of the WCB interacts with the upper-level jet and potentially amplifies the Rossby-wave structure (Grams *et al.*, 2011; Teubler and Riemer, 2016), which can subsequently lead to the development of baroclinic waves (Grams and Archambault, 2016) and atmospheric blocks (Pfahl *et al.*, 2015; Steinfeld and Pfahl, 2019). The correct depiction of WCBs and their outflows in numerical weather prediction (NWP) models is of great importance, as misrepresentations can lead to an incorrect large-scale flow configuration and low forecast skill in the medium range (Martínez-Alvarado *et al.*, 2016; Berman and Torn, 2019; Sánchez *et al.*, 2020). The divergent outflow of WCBs plays a key role in the conceptual upscale error growth mechanism introduced by Zhang *et al.* (2007), as it projects small-scale errors at the convective scale on to the large scale (Grams *et al.*, 2018), where they subsequently grow via baroclinic instability (Baumgart *et al.*, 2019).

Besides this upscale propagation of pre-existing errors, WCBs can also introduce errors into the forecast directly, because their ascent is strongly driven by latent heating from cloud diabatic processes (Wernli and Davies, 1997; Madonna *et al.*, 2014). As these processes are not resolved explicitly by the grid of global NWP models, they are parametrised, acting as a source of forecast error. The parametrisation schemes that contribute the most to the diabatic heating during the ascent of WCBs are the microphysics and convection schemes (Joos and Forbes, 2016). Several studies show that WCBs and their impact
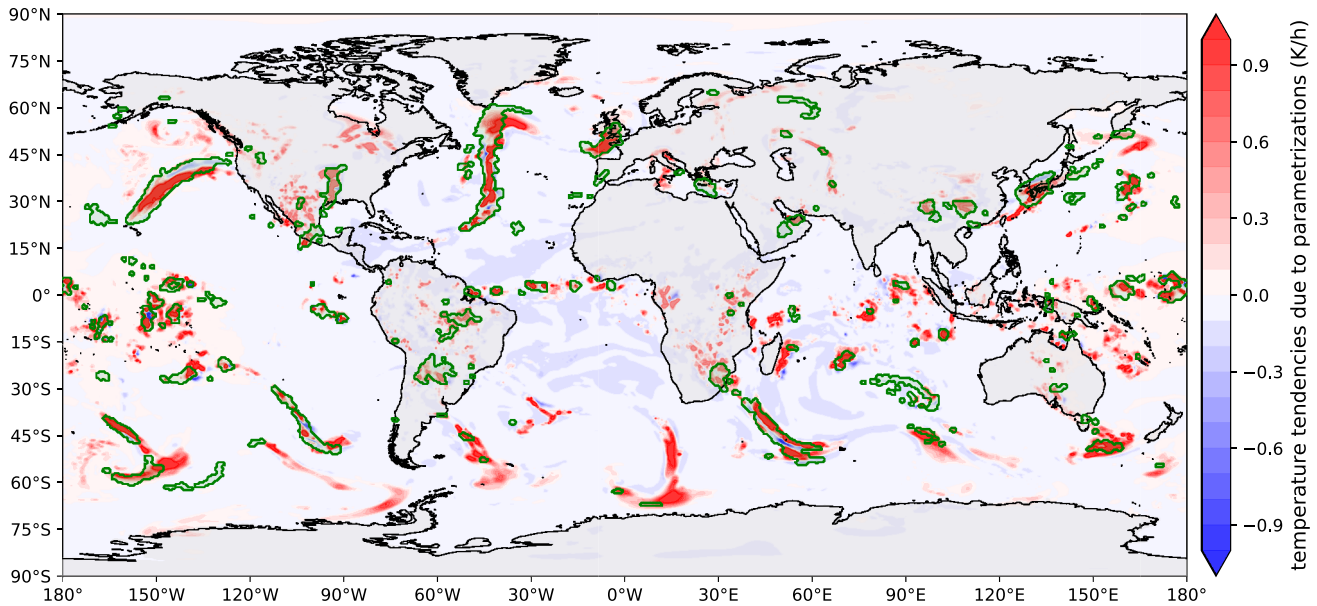
FIGURE 1 One-hr accumulated temperature tendencies due to parametrisations (shading every 0.1 K·h^{-1}) averaged over the model levels 105–96 (approx. 700–500 hPa) from the ERA5 short-term forecast initialised at 1800 UTC on March 8, 2016 at lead time 6 hr and rapidly ascending air streams (ascent of at least 600 hPa in 48 hr) in their ascending stage between 800 and 400 hPa from ERA5 reanalysis data valid at 0000 UTC on March 9, 2016 (green contour), identified by trajectory analysis as explained in Section 2 [Colour figure can be viewed at wileyonlinelibrary.com]

on the upper-level jet stream are sensitive to the choice of parametrisation schemes (Joos and Wernli, 2012; Joos and Forbes, 2016; Maddison *et al.*, 2020; Mazoyer *et al.*, 2021; Rivière *et al.*, 2021), and systematic errors in the upper-level Rossby-wave structure are linked to uncertainties in the parametrisations of diabatic processes (Gray *et al.*, 2014; Martínez-Alvarado *et al.*, 2016). Also other weather systems, such as (recurving) tropical cyclones and mesoscale convective systems, are associated with rapidly ascending air streams and are driven by the release of latent heat. Similarly to WCBs, their diabatic outflow can influence the upper-level midlatitude flow (Grams and Archambault, 2016) and lead to downstream forecast uncertainty (Rodwell *et al.*, 2013; 2018) in the Extratropics.

The SPPT scheme is designed to introduce uncertainty into regions where parametrisations are active, and the magnitude of the perturbation is proportional to the net physics tendency (Leutbecher *et al.*, 2017). Regions with large physics tendencies and hence large perturbations correspond very well to regions where rapid ascending motions occur: Figure 1 illustrates this linkage for one situation in March 2016, where midtropospheric temperature tendencies from all parametrisation schemes (colour shading) are co-located with rapidly ascending air streams associated with WCBs and tropical convection (contours). This study examines how such diabatically driven weather systems are affected by the SPPT scheme, and is organized as follows. The experimental setup and the detection of

rapidly ascending air streams are described in Section 2. In Section 3, the effect of SPPT and initial condition perturbations on rapidly ascending air streams is analyzed in a set of numerical sensitivity experiments in Lagrangian (Section 3.1) and Eulerian (Section 3.2) frameworks, and the impact of SPPT on vertical velocities is linked to changes in precipitation in Section 3.3. Thereafter, operational ensemble forecasts are used to corroborate the main findings of this study (Section 3.4). A discussion of the results is given in Section 4, and concluding remarks and ideas for further research are found in Section 5.

2 | DATA AND METHODS

2.1 | Experimental setup

In order to investigate the effect of SPPT on rapidly ascending air streams, experiments with different ensemble configurations have been conducted. In the reference experiment (REF), both initial condition (IC) and model physics perturbations with SPPT are applied (as in the operational setup). In no-SPPT, only IC perturbations are activated and the model physics remains unperturbed, and vice versa in no-INI, where the forecasts start from unperturbed initial conditions and only SPPT is applied. The IC perturbations are constructed as a combination of an ensemble of 4D-var data assimilations (Buizza *et al.*, 2008) and singular vectors (Leutbecher and Palmer, 2008). The experiments use

TABLE 1 Details about the data sets and trajectory calculation setups

	Sensitivity experiments	Operational data set
Model	IFS CY46R1	IFS CY45R1/CY46R1/CY47R1
Resolution	TCo399L91	TCo639L91
Perturbed members	20	50
Simulation period	August 15–October 15, 2016	December 1, 2018–November 30, 2020
Start interval	48 hr	12 hr
Max. lead time	288 hr (12 days)	288 hr (12 days)
Number of analysis time steps	285	2,961
Trajectory calculation		
Grid spacing of model output	1 × 1°	1 × 1°
Trajectory starting region	Globally	North Atlantic
Trajectory starting points	100-km equidistant grid	100-km equidistant grid
Vertical levels	1,000 to 700 every 25 hPa	1,000 to 700 every 50 hPa
Selection criterion	600 hPa / 48 hr	550 hPa / 48 hr
Tracing of physical quantities	Yes	No

ECMWF's Integrated Forecasting System (IFS) CY46R1 (Haiden, 2019; operational between July 2019 and June 2020) at a spatial resolution of TCo399 (average grid spacing of 29 km; the operational forecasts are run at TCo639) with 91 vertical model levels (model top at 0.01 hPa) and are initialised from ECMWF's operational high-resolution analysis. To compromise between the computational effort and obtaining a sample size that is large enough for statistical analyses, the ensemble size is reduced to 20 perturbed (operational: 50) and one unperturbed member. Overall, 32 forecasts between August 15 and October 15, 2016 are run out to 12 days. The study period during Autumn 2016 has been chosen to match the North Atlantic Waveguide and Downstream Impact Experiment (NAWDEX) field campaign (Schäfler *et al.*, 2018), which aimed at gathering observations from WCB outflow at the tropopause level. The period was characterized by enhanced WCB activity and several extratropical transitions of tropical cyclones in the North Atlantic sector. Subsequent to the measurement campaign, many case studies have been published, mostly combining observations with numerical simulations (see Schäfler *et al.*, 2018 for a detailed overview of the field campaign). Details about the setup of the experiments and how it differs from the operational setup are summarized in Table 1.

2.2 | Trajectory calculation

Rapidly ascending air streams are detected by computing kinematic trajectories based on the 3D wind field on

model levels with the LAGRANTO toolkit (Wernli and Davies, 1997; Sprenger and Wernli, 2015). 48-hr forward trajectories are started globally on a 100-km equidistant grid every 25 hPa between 1,000 and 700 hPa, and a trajectory is subsequently classified as "rapidly ascending" when its pressure decreases by at least 600 hPa in two days. This setup is similar to the one used in Madonna *et al.* (2014) to obtain a global WCB climatology. However, we omitted any further trajectory filtering related to the absence of extratropical cyclones or to double counts of trajectories representing the same air mass for efficiency reasons. Thus the trajectory count is not linearly proportional to air-mass transport, which has to be taken into consideration when interpreting the data. We have analyzed the impact of the double-counting with a reduced data subset and found no qualitative change in the interpretation of our results. The trajectory computations were implemented parallelised into an automated postprocessing suite, which enables the detection of rapidly ascending air streams in all ensemble members of the three experiments, REF, no-SPPT, and no-INI, without the need to store large amounts of data offline. Further, 2D masks are computed from the Lagrangian trajectories: all 1x1° grid cells that are touched or enclosed by a circle with a radius of 100 km around the trajectory point are assigned the value 1 at the corresponding valid time. This procedure is done separately for air parcels residing in an inflow (below 800 hPa), ascent (between 800 and 400 hPa), or outflow (above 400 hPa) layer. An example for gridded trajectories in their ascent stage is shown as contours in Figure 1.

Sensitivity tests for one case study revealed that the trajectory calculation is sensitive to the grid spacing of the interpolated output fields as well as to the time interval. A higher resolution of the grid and a shorter time interval between the input fields results in higher trajectory numbers surpassing the threshold of 600 hPa within two days. This has been tested for 1°, 0.5°, and 0.25° grids and 6-, 3-, and 1-hr time intervals, with the largest trajectory count for the combination of 0.25° and one-hourly fields and the lowest count for 1° and six-hourly fields (factor of about 2.5 between the setups in a representative case study). This behaviour is likely an effect of double-counting of trajectories, which becomes more relevant when the (temporal) resolution of the input fields is higher. However, we found that the relative impact of SPPT on the diagnostics used in this study does not depend on the setup of the trajectory calculation (not shown). Therefore, the analysis presented here is based on 1° and six-hourly data (see Table 1). Further, the case study revealed that the native model resolution does not change substantially the number of trajectories fulfilling the ascent criterion (tested for TCo399, TCo639, and TCo1279; not shown), and, more importantly, the relative impact of SPPT on the trajectory count is not sensitive to model resolution. For efficiency reasons, we therefore use the TCo399 setup.

2.3 | Verification data sets

The systematic verification of Lagrangian flow features, such as WCBs, is challenging, as they cannot be compared directly with observations. Instead, trajectories in forecasts are usually evaluated by computing the same diagnostics in a comparable (re)-analysis data set (e.g., Madonna *et al.*, 2015; Grams *et al.*, 2018). For this study, three different reference data sets have been tested, all at a six-hourly temporal resolution: ECMWF's operational high-resolution (TCo1279) analysis, which is based on four-dimensional variational data assimilation (4D-VAR: Rabier *et al.*, 2000); the ERA5 reanalysis (Hersbach *et al.*, 2020); and the operational high-resolution analysis interpolated to the grid (horizontal and vertical) of the ensemble experiments. The interpolation that is used for the latter is the same that is used to interpolate initial conditions for the forecast model (ECMWF, 2019). Qualitatively, the three data sets agree well regarding the trajectory-related diagnostics, even though there are some differences between ERA5 and the two data sets based on the operational analyses (especially in the Tropics; not shown). As the interpolated analysis is technically the most coherent with the experiments, we chose to use it as reference data set, and refer to it as "interpolated analysis" (ANA). Nevertheless, it is important to note that this data set is only an estimate of the true state of the atmosphere and might have deficiencies regarding the characteristics of rapidly ascending air streams.

2.4 | Operational data set

To test the sensitivity of the results to the chosen simulation period and to the experimental setup, trajectories computed from two years (December 1, 2018–November 30, 2020) of operational forecasts of ECMWF's ensemble prediction system are also analyzed. The operational ensemble is run at a higher resolution (TCo639) than the experiments (TCo399) and consists of 50 perturbed (SPPT and IC perturbations) and one unperturbed control member. The available data set contains only trajectories in the North Atlantic sector, and the trajectory computation differs slightly from the one used for the experiments (see Table 1). However, the results presented here are not affected by these differences. It is nontrivial to recompute trajectories for this period, as the computation relies on real-time model level data, which are not archived in the long-term Meteorological Archival and Retrieval System (MARS) at ECMWF. For more details about the differences of the experimental and operational setups, see Table 1.

3 | RESULTS

In this section, we present the results of the study. First, we apply the trajectory-based diagnostics described in Section 2 to the sensitivity experiments to quantify the effect of SPPT on rapidly ascending air streams (Section 3.1). Then, an Eulerian framework is adopted (Section 3.2), followed by an analysis on the effect of SPPT on precipitation (Section 3.3). Finally, the main findings from the experiments are corroborated by analyzing trajectories from operational ensemble forecasts (Section 3.4).

3.1 | Lagrangian perspective

3.1.1 | Gridded frequencies

Figure 2a shows the mean gridded frequencies of trajectories reaching the upper troposphere above 400 hPa during the simulated period in the interpolated analysis (ANA). The threshold of 400 hPa reflects the outflow stage of WCBs in the Extratropics (e.g., Madonna *et al.*, 2014) and other diabatically enhanced air streams (termed "diabatic outflow" or simply "outflow" in the following, cf. Grams and Archambault, 2016). In the Northern Hemisphere Extratropics, two regions of enhanced diabatic outflow
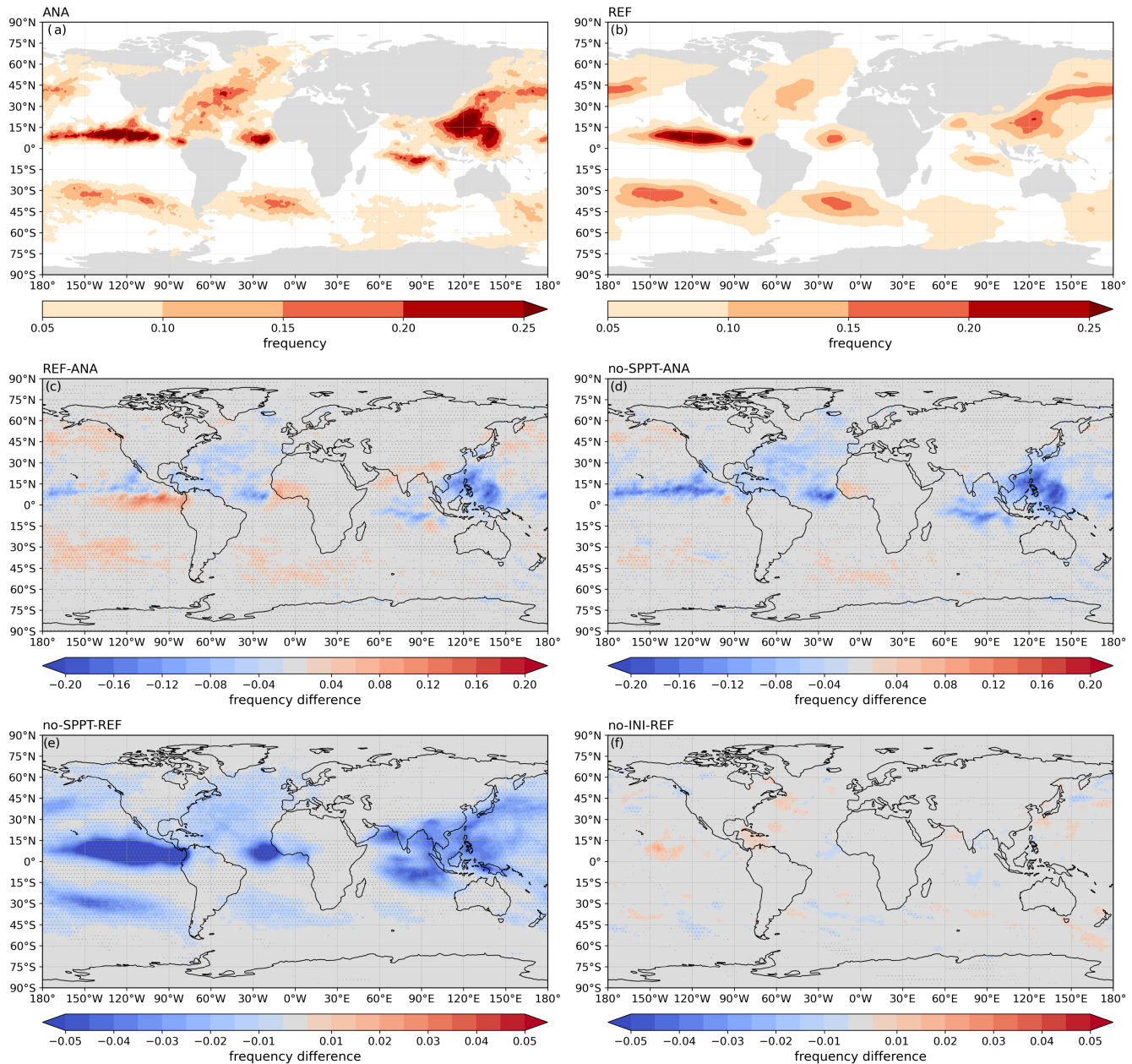
FIGURE 2 Frequency maps of trajectories reaching the upper troposphere above 400 hPa (a) over all analysis times (285 time steps) for the interpolated analysis, (b) over all forecasts (32), lead times (41), and ensemble members (20) for experiment REF, (c) the difference between REF and the interpolated analysis, (d) the difference between no-SPPT and the interpolated analysis, (e) the difference between no-SPPT and REF, and (f) the difference between no-INI and REF. The stippling in (c)–(f) denotes statistically significant differences between the data sets at a confidence level of 0.99 based on a χ^2 test. Note that the displayed differences refer to absolute differences of the frequencies [Colour figure can be viewed at wileyonlinelibrary.com]

are visible in the storm tracks of the North Atlantic and North Pacific, with maximum frequencies of up to 20% in the North Atlantic and up to 15% in the North Pacific. Enhanced outflow is also present in the South Pacific and Atlantic basins, with overall lower frequencies than in the Northern Hemisphere. Additionally to these typical WCB regions, the Tropics also show enhanced frequencies of diabatic outflow, especially the tropical Pacific and Atlantic, with widespread regions exceeding frequencies

of 25%. Due to the global distribution of trajectory starting points, rapidly ascending air streams related to tropical convection and tropical cyclones are also detected (and not only WCBs).

The outflow frequencies of the reference simulation REF, computed over all forecast initialisations, lead times, and members, resemble the patterns from the analysis, even though the fields are much smoother due to the 20-member ensemble (Figure 2b). However, the difference

between REF and ANA reveals that REF underestimates the outflow frequencies in the North Atlantic sector as well as in most parts of the Tropics, especially over the Maritime Continent (Figure 2c). In the extratropical North Pacific and the Southern Hemisphere storm tracks, the outflow frequency is overestimated by REF. Figure 2d shows that deactivating SPPT leads to improved outflow frequencies where REF has too much outflow, while the simulations with activated SPPT perform better in regions where the frequencies are underestimated by the model (e.g., in the North Atlantic and the Tropics).

The comparison of no-SPPT and REF reveals that the outflow frequency is systematically reduced globally without model uncertainty representations through SPPT (Figure 2e). The reduction is largest in the regions where the absolute frequencies are highest, that is, in the tropical regions (exceeding 5%) and in the North Atlantic and Pacific (2–4%). The sign of the signal is negative everywhere except for a few grid points at high latitudes in regions with very low absolute frequencies. Hence, the reduced frequencies in no-SPPT compared with REF are systematic. The comparison of REF and no-INI reveals that no systematic frequency changes are introduced by the IC perturbations (Figure 2f).

3.1.2 | Trajectory counts

To investigate further the differences between the experiments, the number of trajectories in different regions of the globe are counted. The regions are chosen to separate tropical (tropical convection) from extratropical trajectories (WCBs). Further, a special focus is set on the North Atlantic, as it is a very prominent WCB region impacting European weather. A trajectory is assigned to a region when its starting position lies within the boundaries of the region, which are indicated in Table 2. The counts are normalized by the maximum possible number of trajectories in each region. Therefore, the numbers of different regions are directly comparable, as they do not rely on the size of the region.

Note that trajectory counts in these regions are not directly comparable to the frequencies at the corresponding grid points. The calculation of the Eulerian frequencies is based on a gridding algorithm, which assigns the value 1 to a grid point when a trajectory is detected within the radius of influence (here 100 km) or 0 if no trajectory is detected (see Section 2.2). Therefore, this method does not account for the trajectory density at one single grid point, which might be higher when multiple trajectories impact a specific grid point.

The distributions of the normalized trajectory counts over all forecasts, lead times, and perturbed members in

TABLE 2 Boundaries of regions for which trajectory characteristics are computed

Region	Abbreviation	Region boundaries
Global	G	−180°–180° E, −90°–90° N
Global Tropics	TROPICS_G	−180°–180° E, −20°–20° N
Northern Hemisphere Extratropics	NH_ET	−180°–180° E, 30°–90° N
North Atlantic	NATL	−70°–10° E, 25°–65° N

all regions are depicted in Figure 3. Globally, the median trajectory count in no-SPPT is around 37% less than in REF. In absolute numbers, this is a reduction from around 2009 trajectories in REF to 1271 in no-SPPT per time step. In the Tropics, the difference between the medians is much larger (reduction by 60%), while the effect is less prominent in the Extratropics (21% in the Northern Hemisphere Extratropics and 32% in the North Atlantic). Trajectory counts in no-INI do not differ from the ones in REF; not only the medians, but also the distributions agree very well, showing that IC perturbations do not systematically affect the occurrence of WCBs. Moreover, the median counts of the unperturbed control member (dashed lines) are indistinguishable from the medians of no-SPPT.

The variability in the different regions depends strongly on the size of the region: globally and in the Tropics, the variability is very low, as there are always subregions with enhanced vertical velocities on the globe. In the smaller North Atlantic domain, WCB activity depends on single transient weather systems. Hence, the lower edge of the distribution has the value 0, as there are situations without any trajectories fulfilling the ascent criterion in the domains. On the other hand, synoptic situations with strong WCB activity lead to much higher relative trajectory numbers in the smaller regions. Additionally, the reduced sample size in the smaller regions leads to larger variability.

Note that the differences in the trajectory counts are given in relative numbers, whereas the differences of the gridded frequencies in Figure 2 are expressed as absolute values. Thus, qualitatively both approaches show the same picture and are of the same order of magnitude. Remaining quantitative differences are due to the trajectory-gridding algorithm described above. The trajectory count diagnostic used here, however, does not allow for a direct quantification of air-mass transports from the lower to the upper
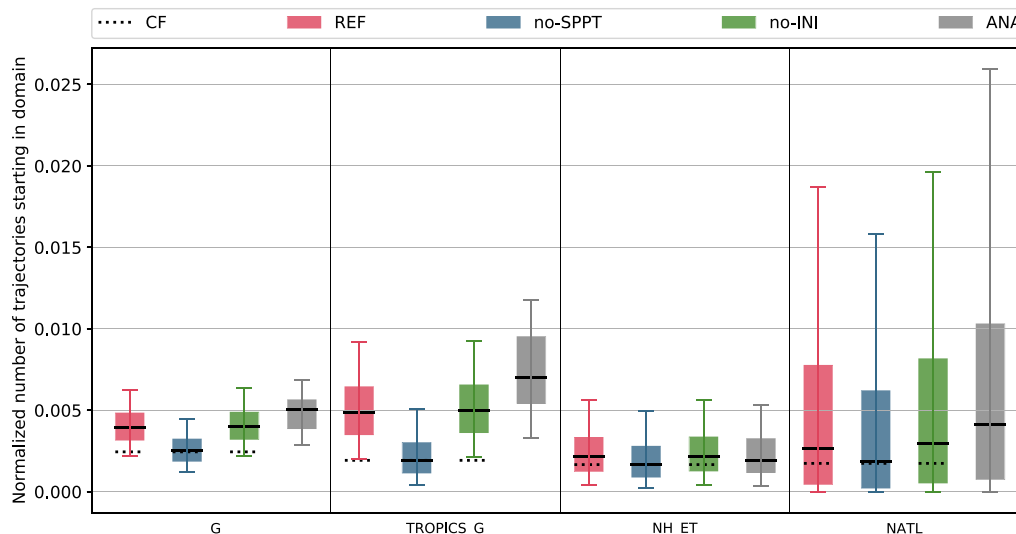
FIGURE 3   Trajectory counts starting in the global domain (G), the tropical belt (TROPICS_G), the Northern Hemisphere Extratropics (NH_ET), and the North Atlantic sector (NATL) for the experiments REF, no-SPPT, no-INI, and the interpolated analysis (ANA). Counts are normalized by the maximum number of possible trajectories in each domain (i.e., all trajectories before the selection procedure). The solid line is the median of the distribution, the boxes denote the interquartile range and whiskers the 5–95 interquantile range. The dashed line is the median of the unperturbed control member (CF) [Colour figure can be viewed at wileyonlinelibrary.com]

troposphere, because no double-counting filter has been applied (see Section 2.2).

The median trajectory counts of the unperturbed control member (CF) are identical to the ones in no-SPPT in all regions. This is expected, as the control member does not see any stochastic physics perturbations and the IC perturbations do not influence rapidly ascending air streams systematically. Nevertheless, this is very useful information, because most modelling centres issue an unperturbed forecast as part of their operational ensemble forecast. Therefore, studies investigating some of the effects of model uncertainty schemes may not necessarily rely on expensive experiments, but could also be conducted by exploiting operational ensemble forecasts.

The systematic increase of rapidly ascending air streams by SPPT raises the question of whether the NWP model with unperturbed or perturbed physics produces a better representation of WCBs compared with a verifying analysis. To investigate this, the same trajectory count diagnostic has been applied to the interpolated analysis. Globally, all experiments underestimate the occurrence of rapidly ascending air streams during the period investigated, compared with the interpolated analysis. This underestimation arises predominantly from the Tropics, where the trajectory counts are strongly reduced in the experiments. Also, in the North Atlantic the experiments simulate too few rapidly ascending air streams. In contrast, the trajectory counts are slightly overestimated in the Northern Hemisphere Extratropics. As SPPT systematically increases the trajectory count, the offset between

the simulations and the interpolated analysis is increased in the experiments without SPPT in regions where the trajectory counts are underestimated by REF (Tropics, North Atlantic). In regions where the counts are overestimated by REF (Northern and Southern Hemisphere Extratropics), the deactivation of SPPT makes the trajectory frequencies more consistent with the interpolated analysis. Due to these regional differences, a general statement on whether SPPT improves or deteriorates the representation of rapidly ascending air streams cannot be made.

The number of trajectories decreases with lead time in all experiments (Figure 4; note that the time axis corresponds to the time of the trajectory start). This explains the reduced trajectory counts in most parts of the globe, compared with the verifying analysis. In the global domain, starting at a level close to the counts in the interpolated analysis, the number of trajectories in REF and no-INI decreases rapidly by about 25% during the first 48 hr of the forecast and then stays constant. The counts in the no-SPPT experiment show a very similar behaviour, but the curve has an offset to lower values. The number of trajectories in the simulations decreases with lead time and consequently the underestimation compared with the analysis increases. This lead-time dependence is similar in the other regions investigated and shown as an example for the Northern Hemisphere Extratropics (dotted lines). In that region, however, the simulations with perturbed model physics initially overestimate the trajectory counts and level off close to the interpolated analysis at later lead
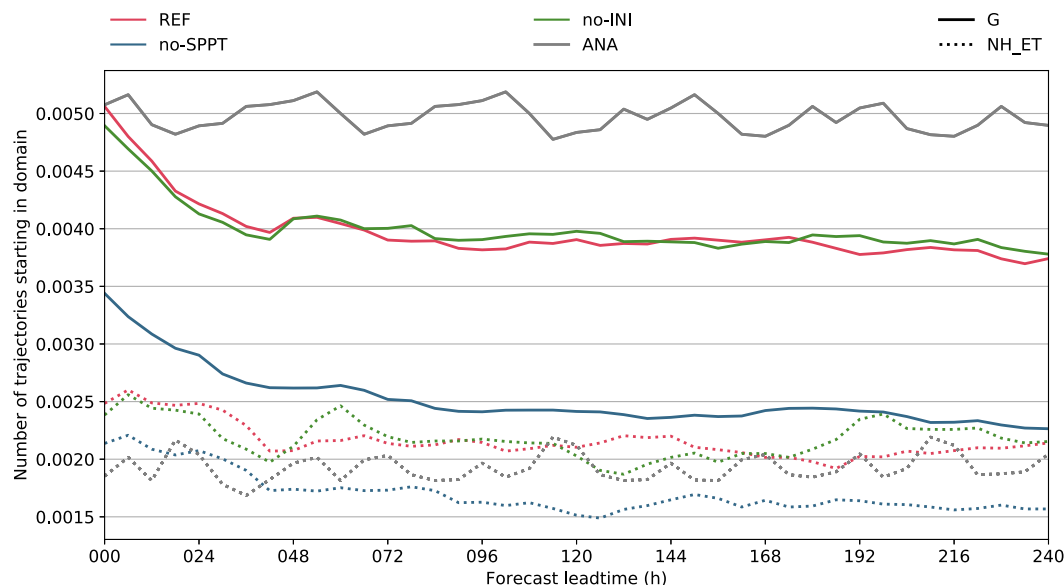
FIGURE 4 Medians of trajectory counts starting in the global (G, solid lines) and Northern Hemisphere extratropical domains (NH_ET, dashed lines) with forecast lead time, normalized by the maximum number of possible trajectories in each domain, of the experiments REF, no-SPPT, no-INI, and the interpolated analysis (ANA). The time axis corresponds to the time of the trajectory start [Colour figure can be viewed at wileyonlinelibrary.com]

times, while no-SPPT initially matches the analysis and drops below it during the forecast integrations.

The differences between simulations with perturbed physics (REF and no-INI) and no-SPPT stay almost constant with lead time. This indicates that SPPT influences the ascending air streams directly and does not change the mean state during the course of the forecast. If the deviation was time-dependent (i.e., very small or nonexistent in the beginning and increasing with forecast lead time), it would suggest that the perturbations alter the atmospheric state in a way favourable for the development of rapidly ascending air streams during the forecast, such as moisture accumulation in the boundary layer.

3.1.3 | Trajectory characteristics

As SPPT systematically changes the frequency of rapidly ascending air streams, the question arises of whether stochastic perturbations also influence their physical properties and characteristics. The Lagrangian perspective allows for the calculation of the evolution of meteorological fields along the trajectories. In this section, we focus on the latent heating rate of the trajectories, mainly for two reasons: firstly, because the intense latent heat release in the ascending air streams is the reason why the SPPT scheme affects them, and, secondly, because the diabatic heating lifts the air parcel cross-isentropically and is therefore a key parameter, which determines the height of the outflow and its impact on the large-scale circulation.

Figure 5 shows the frequency counts of latent heating rates (i.e., difference between maximum and minimum potential temperature) of all detected trajectories within the regions listed in Table 2. The distribution in the global domain shows that all analyzed trajectories are heated by at least 10 K, which emphasizes the importance of diabatic processes for these ascending air streams. The global distribution of latent heating rates is dominated by two regimes in all experiments: one with a maximum occurrence centred around 45 K, and another one at lower values between 20 and 35 K. By looking at the other regions, it becomes clear that the regime associated with larger values is strongly dominated by the Tropics, while the regime with lower heating rates is represented more by the extratropical regions. However, the heating rates in the Northern Hemisphere Extratropics and in the North Atlantic are mostly characterized by values that lie in between the two distinct global regimes, indicating that the lower heating regime is not explicitly depicted by the selected regions, and predominantin,for example, the Southern Hemisphere storm tracks (not shown).

Comparing the global frequency counts of no-SPPT and REF shows that the median heating rate is strongly reduced when SPPT is deactivated (reduction of 7 K). However, the shapes of the histograms indicate that no-SPPT primarily underestimates the frequency of strongly heated trajectories in the upper regime, while the frequencies of the less heated trajectories are similar in REF and no-SPPT. Splitting the trajectories into subregions makes the distributions more comparable. In the Tropics, the median
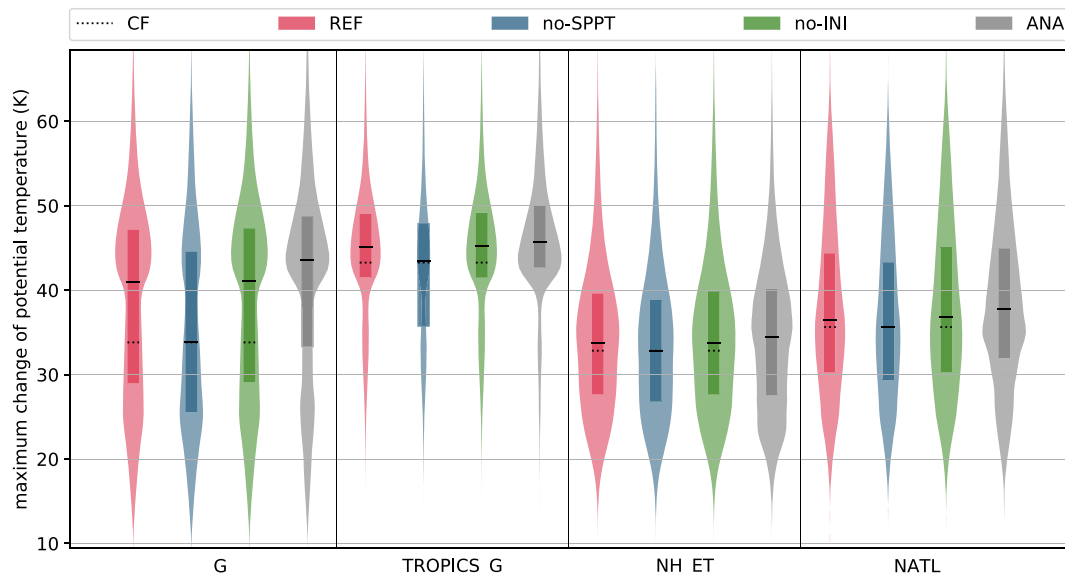
FIGURE 5   Frequency distributions of latent heating rates along trajectories starting in the global (G), tropical (TROPICS_G), Northern Hemisphere extratropical (NH_ET), and North Atlantic (NATL) domains for the experiments REF, no-SPPT, no-INI, and the interpolated analysis (ANA). The black lines indicate the median and the boxes the interquartile ranges of the distributions. The dotted line represents the median value of the unperturbed control member. The scales of the frequency distributions are identical for all experiments within each region, allowing for a quantitative comparison between the experiments [Colour figure can be viewed at wileyonlinelibrary.com]

difference between REF and no-SPPT is about 1.5 K, and in the Northern Hemisphere Extratropics and in the North Atlantic it is about 1 K. Comparing the simulated heating rates in the different regions with the interpolated analysis shows a similar effect to that for the trajectory count: heating rates are underestimated globally by all experiments, but SPPT leads to a more realistic representation compared with simulations with unperturbed physics. The medians of the unperturbed control member (CF) again resemble the ones from no-SPPT, and the distributions of no-INI are very similar to the ones of REF. This corroborates the inferences from the trajectory count diagnostics regarding the potential use of the control member from operational forecasts.

A more physical classification is to assign the trajectories to one of the two global heating regimes, independent of their origin. The local minimum between the two heating maxima lies approximately at the value of 38 K in REF (Figure 5); hence, this value is chosen as the threshold to classify each trajectory into either the upper or lower category. For each of the two regimes, several characteristics have been computed, and the trajectory counts and heating rates are shown in Figure 6. For the lower heating rates, the deviation of the trajectory count in no-SPPT from REF is much smaller (11%) than for higher heating rates (52%; Figure 6a). Comparing the experiments with ANA shows that the trajectory count is slightly overestimated in the lower heating regime, with a larger positive bias in the experiments with SPPT than those without SPPT,

while it is strongly underestimated in the upper heating regime, where the experiments with SPPT are closer to ANA than those without SPPT. The temporal evolution of the trajectory counts (Figure 6c) illustrates that the number of strongly heated trajectories drops rapidly during the first two days of the forecast, and SPPT helps to keep the counts closer to ANA. In contrast, the number of less heated trajectories is maintained throughout the forecast, and no-SPPT accurately represents the counts of ANA, while the experiments with SPPT overestimate the counts.

Substantially different behaviour between the two heating regimes is not observed for the characteristics of the trajectories. The difference in latent heating between REF and no-SPPT is very small and does not depend on the heating regime (Figure 6b). Table 3 summarizes the median values of trajectory characteristics (trajectory count, latent heating rate, isentropic and isobaric outflow level, and specific humidity at trajectory start) derived from the trajectories and gives an overview of the effects of SPPT on different aspects of rapidly ascending air streams in the two heating regimes. Similarly to the heating rates, the trajectory characteristics are only changed marginally or even remain unchanged when SPPT is activated. For example, the minimum pressure of the trajectories increases by 1.7 hPa in the lower regime and decreases by 1.5 hPa in the upper regime when SPPT is deactivated.

The large difference between the heating rates in REF and no-SPPT (see Figure 5) is therefore mainly a result of changed trajectory frequencies in the different
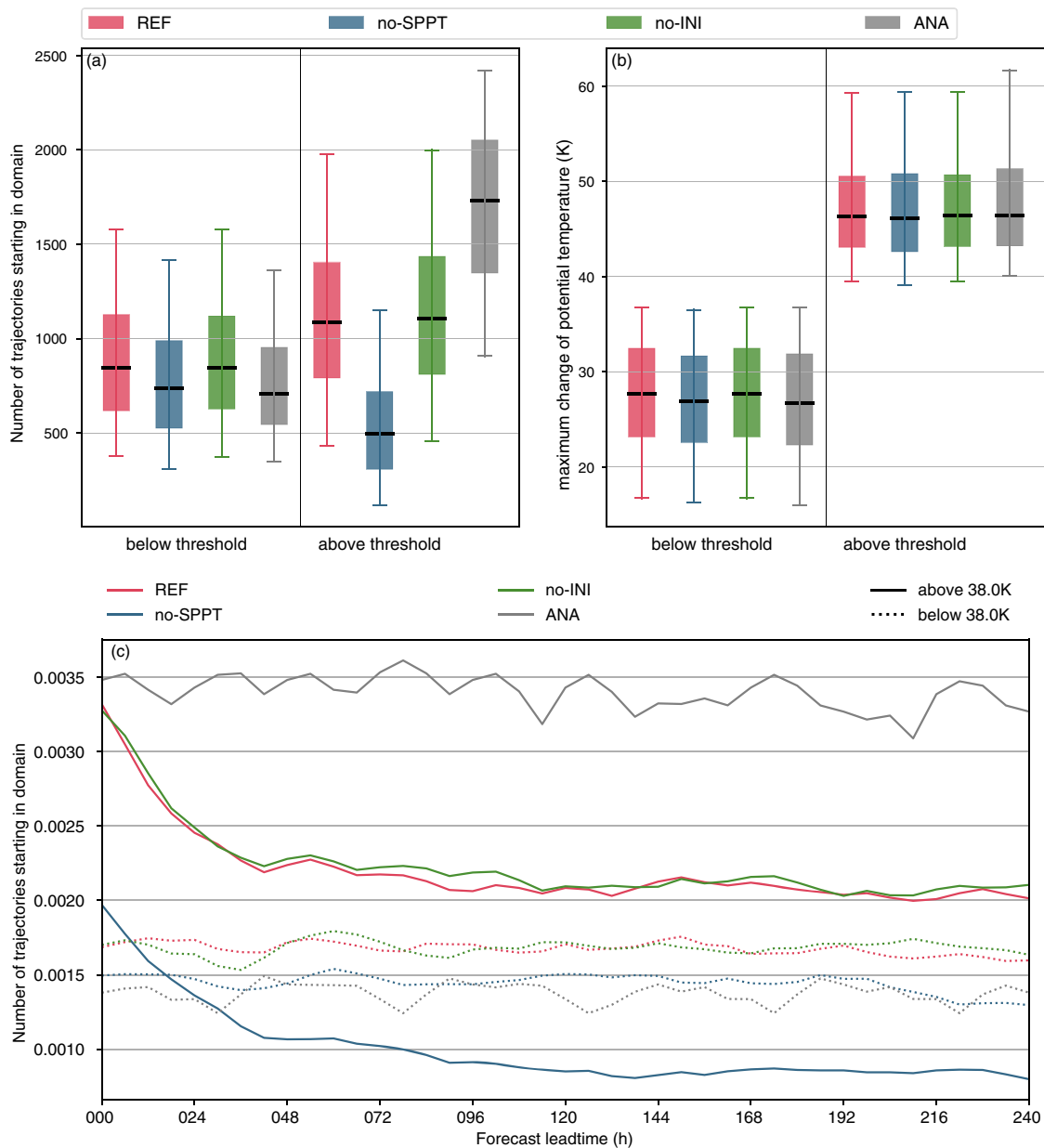
FIGURE 6 (a) Trajectory count, (b) latent heating rate, and (c) trajectory count as a function of forecast lead time of all trajectories (global) in the experiments REF, no-SPPT, no-INI, and the interpolated analysis (ANA), separated for the two latent heating regimes below (left) and above (right) the threshold of 38 K [Colour figure can be viewed at wileyonlinelibrary.com]

regions. Globally, rapidly ascending air streams occur more frequently with SPPT than without, and this effect is stronger for large heating rates than for small heating rates. Hence, the global statistics of trajectory characteristics will take the shape of stronger heated air streams, which results in larger heating rates and outflow heights (not shown). Also, regionally (e.g., in the North Atlantic sector), SPPT increases the WCB frequency more strongly in the (sub)tropical part of the domain than in the poleward part. However, comparing trajectories with similar heating rates (and not based on their origin) shows that

individual trajectories are not substantially modified by SPPT. This is in agreement with the conclusions drawn from Figure 4: SPPT does not change the environmental conditions of rapidly ascending air streams or affect the trajectory characteristics significantly, but acts directly on ascending motions and helps to initiate rapid ascents.

Even though the physical properties of the trajectories do not differ substantially, the latent heating rates help to differentiate between strongly and weakly heated trajectories. The frequency of strongly heated rapidly ascending air streams is generally underestimated in the experiments

TABLE 3 Median values of various variables calculated along trajectories for two heating regimes: "Lower", with latent heating rates below 38 K, and "Upper", with latent heating rates above 38 K for the experiments REF, no-SPPT, no-INI, and the interpolated analysis (ANA)

| Variable	Heating regime	REF	no-SPPT	no-INI	ANA
Trajectory count	Lower	851	735	854	707
	Upper	1109	497	1129	1729
Latent heating rate (K)	Lower	27.7	26.9	27.7	26.7
	Upper	46.4	46.1	46.5	46.4
Isentropic outflow level (K)	Lower	324.6	323.7	324.7	323.7
	Upper	349.4	349.9	349.5	349.7
Outflow pressure (hPa)	Lower	288.1	289.8	288.0	291.6
	Upper	206.4	204.9	205.8	201.8
Inflow specific humidty (g·kg^{-1})	Lower	11.2	11.0	11.2	10.7
	Upper	14.9	15.1	14.9	15.1

compared with the analysis, while the trajectories in the lower heating regime are slightly overestimated. Therefore, by increasing the frequency of rapidly ascending air streams, SPPT makes the trajectory counts more consistent with ANA in the upper heating regime and less consistent in the lower heating regime.

3.2 | Eulerian omega perspective

The trajectory-based analysis in the previous section helps us to detect and understand the sensitivities of rapidly ascending air streams to the perturbations introduced by SPPT. However, the analyzed trajectories consider only the most rapid ascents and therefore cover only a very small fraction of the whole spectrum of (upward) vertical velocities. The slowest vertical velocity that is needed to fulfil the ascent criterion of 600 hPa within two days corresponds to a constant 0.35 Pa·s^{-1}, but about 95% of the midtropospheric upward velocities are slower than this threshold (REF experiment; Figure 7a). Additional to this scale sensitivity, only (net) upward velocities can be detected by the trajectory diagnostics and instantaneous downward motion is not considered at all. In order to take into account the slower upward velocity scales as well as downward motion, distributions of midtropospheric (i.e., at 500 hPa) vertical velocities for all forecasts, lead times and perturbed ensemble members are computed based on all grid points in the global domain G (Figure 7a). The shape of the frequency distributions indicates that slow velocities occur far more often than fast velocities (note the logarithmic scale) and that ascending (negative omega) motions are typically faster than descending (positive omega) motions (skewed distribution).

Comparing the distributions among the experiments shows that no-SPPT has fewer occurrences of fast upward velocities in the range from −3 to −0.5 Pa·s^{-1} compared with REF (Figure 7a). This reflects the reduced number of trajectories fulfilling the ascent criterion of 600 hPa in two days shown in the previous section. However, the effect of deactivating SPPT on upward velocities of smaller magnitude is differential (Figure 7b): very slow ascents (between −0.1 and 0 Pa·s^{-1}) are reduced, while moderate ascents (between −0.5 and −0.1 Pa·s^{-1}) occur more often without SPPT. Despite the large absolute difference of grid points with vertical velocities in the interval between −0.5 and 0 Pa·s^{-1}, the relative differences (dashed line in Figure 7b) are much smaller (−1% to 1%) than for faster upward velocities (up to 50%). On the positive side of the spectrum, no-SPPT uniformly has fewer descending motions throughout the whole range of values compared with REF.

This Eulerian diagnostic using instantaneous fields of omega helps us to understand that not only are very rapid upward motions affected (i.e., a higher number of rapidly ascending trajectories), but all scales of vertical motion are influenced by SPPT. Similarly to rapid ascents, downward motions are enhanced systematically by SPPT. These changes in the descending part of the omega spectrum could be a consequence of the altered upward motions and likely occur for reasons of mass balancing. This hypothesis is motivated by the assumption that ascending motions are much more often connected to parametrised processes (e.g., convection, condensation) than descending motions (e.g., adiabatic descent), for which reason SPPT introduces larger perturbations into regions of ascent than into regions of descent. The reduced occurrence of slow upward velocities between −0.5 and −0.1 Pa·s^{-1} with SPPT could therefore also be a response of the model to the
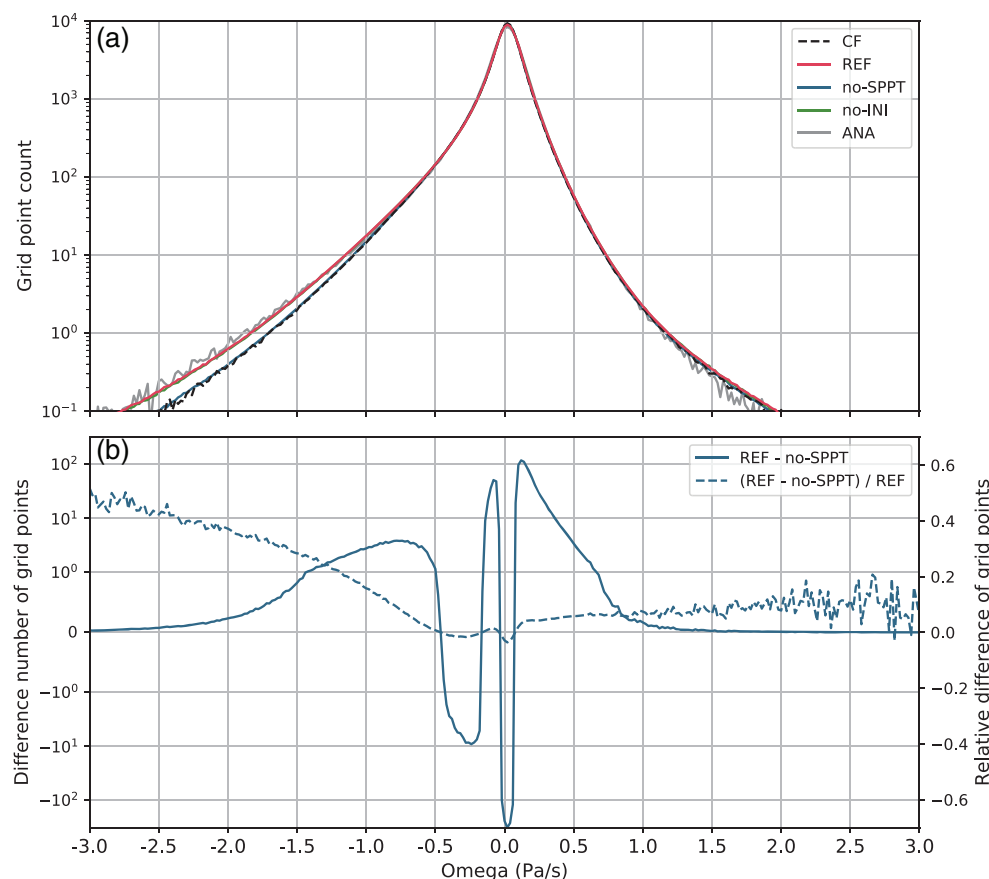
FIGURE 7 (a) Histogram of global (G) vertical velocities at 500 hPa in bins of width $0.02\ \text{Pa·s}^{-1}$ per forecast, lead time, and ensemble member for the experiments REF, no-SPPT, and no-INI, the unperturbed control member (CF), and the interpolated analysis (ANA). (b) Absolute (solid, left axis) and relative (dashed, right axis) differences between the histograms of REF and no-SPPT in panel (a). Negative (positive) omega values correspond to upward (downward) motion. Note that the left y-axis has a linear scale for values between -1 and 1, and a log scale for values smaller than -1 and larger than 1 [Colour figure can be viewed at wileyonlinelibrary.com]

increased fast upward velocities in order to balance the mass fluxes.

The results shown here are consistent with the previous results regarding the trajectory counts: all simulations underestimate upward velocities of large magnitude compared with the interpolated analysis, but experiments with activated SPPT agree better with ANA than no-SPPT; IC perturbations do not alter the omega distributions systematically (almost hidden line in Figure 7a); and the omega distribution of the unperturbed runs (CF) is indistinguishable from that of no-SPPT (dashed line in Figure 7a).

## 3.3 | Impact on surface weather: precipitation

The previous sections have shown that SPPT alters the vertical velocities of the model, resulting in more frequent occurrences of tropical convection and WCBs than in simulations without model physics perturbations. This raises the question of whether other meteorological variables that are linked to rapidly ascending air streams are also affected by these changes. On synoptic timescales, ascending motions in the atmosphere are tied directly to the formation of precipitation, and both tropical convection and

WCBs are weather systems that produce large amounts of precipitation (e.g., Jiang and Zipser, 2010; Pfahl *et al.*, 2014). We therefore examine how precipitation is affected by SPPT, and if this can be attributed to the described changes of vertical motions.

Analogous to the evaluation of vertical velocities in the previous section, the frequency counts of precipitation have been computed for the different experiments. The difference in the histograms between REF and no-SPPT reveals that very small ($<0.5\ \text{mm·hr}^{-1}$) and large precipitation rates ($>1.8\ \text{mm·hr}^{-1}$) occur more often with SPPT than without SPPT (Figure 8). In contrast, precipitation rates between 0.5 and $1.8\ \text{mm·hr}^{-1}$ are reduced by SPPT. The relative change in the number of grid points is particularly apparent for high precipitation rates above around $4\ \text{mm·hr}^{-1}$, with an increase of frequency well above 20%.

These frequency changes are consistent with the impact of SPPT on vertical velocities: differences between REF and no-SPPT of precipitation-rate frequencies strongly resemble the signal corresponding to the upward side of the omega frequency changes in Figure 7b. Rapid ascents that produce large amounts of precipitation occur more often with than without SPPT, while intermediate ascents with smaller precipitation rates are reduced. Accordingly, the precipitation sums associated with the trajectory-based regions of rapid ascents are increased

FIGURE 8 Absolute (solid, left axis) and relative (dashed, right axis) differences between the frequency counts of precipitation rates (bin width of 0.1 mm·hr^{-1}) of REF and no-SPPT per forecast, lead time, and ensemble member (analogous to Figure 7b). The left y-axis has a linear scale between values -1 and 1, and a log scale for values between -1 and 1 [Colour figure can be viewed at wileyonlinelibrary.com]
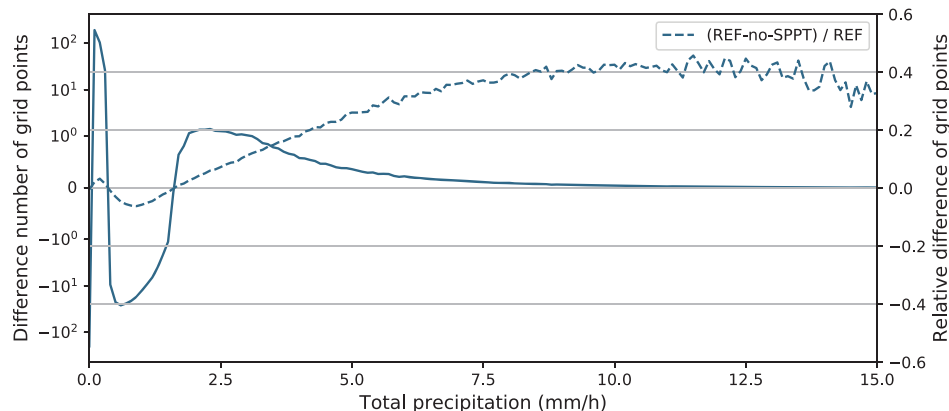
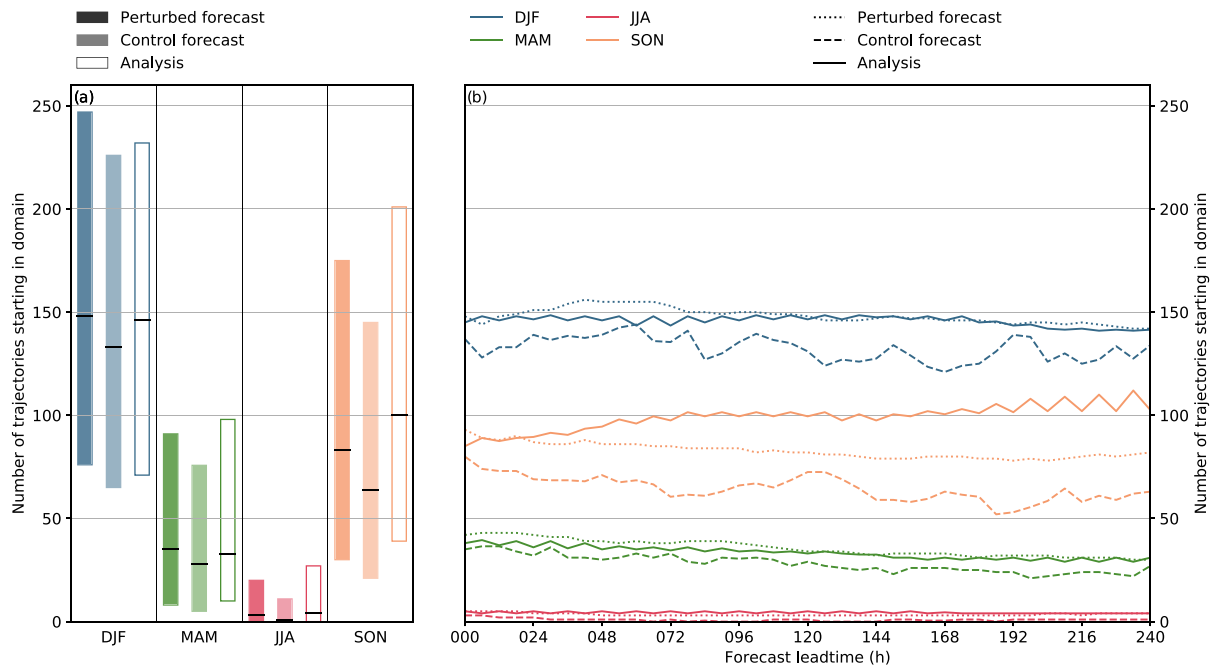## 3.4 | Exploiting operational ensemble forecasts

As shown in the previous sections, unperturbed runs (i.e., the control member in operational forecasts without initial conditions and model physics perturbations) of ECMWF's ensemble prediction system behave similarly to research experiments without stochastic physics perturbations regarding rapidly ascending air streams. These findings can be exploited to investigate the effects of stochastic physics perturbation schemes by comparing the perturbed ensemble members with the unperturbed control member in operational forecasts, avoiding the necessity of expensive sensitivity experiments when investigating longer time periods.

We use this to test the robustness of the results obtained from the experiments by exploiting a data set containing WCB trajectories from operational ECMWF ensemble forecasts from December 1, 2018–November 30, 2020. The setup for the trajectory calculation differs slightly from the one used for the experiments, with the main differences that trajectories are only started in the North Atlantic region (see Table 1) and no physical quantities (e.g., potential temperature to determine the latent heating rate) are evaluated along the trajectories. Further, the operational ensemble runs with 50 perturbed members and at a horizontal resolution of about 18 km (TCo639; see Table 1).

From the operational data set, trajectory counts have been computed in the North Atlantic region similarly to for the experiments, and are split up into seasons according to forecast initialisation date (Figure 9). The seasonal cycle with the highest frequencies in winter and autumn and reduced frequencies in spring and summer arises from a stronger baroclinicity and concomitant cyclone activity in the North Atlantic in the cold season (Madonna

et al., 2014). The comparison of the perturbed and control members reveals that the unperturbed forecasts have a lower median number of WCB trajectories throughout the year compared with the perturbed members (Figure 8a). With activated SPPT, median values increase by 10% in winter and by about 20% in spring and autumn; in summer, the WCB frequency in the North Atlantic is very low, and the relative changes are not meaningful. The offset between the perturbed and unperturbed members depends on the season investigated, with larger relative deviations in autumn and spring, where latent heating rates are larger than in winter. Comparing the medians of the operational high-resolution analysis (unfilled boxes in Figure 9a) with the ones from the forecasts reveals that the difference is larger in the unperturbed forecasts than in the perturbed forecasts. In winter and spring, the perturbed forecasts overestimate the WCB count slightly (1% and 6%, respectively), while the unperturbed members underestimate the frequencies compared with the analysis (9% in winter and 15% in spring). In autumn, both the perturbed and unperturbed members underestimate the trajectory count, but the offset of the unperturbed members is much larger (36%) than that of the perturbed forecasts (17%).

The evolution of the trajectory counts with lead time also differs from season to season (Figure 9b). In the transition seasons (i.e., spring and autumn), the trajectory counts of the operational analysis (solid lines) are not independent of the forecast lead time, because later lead times are closer to the subsequent season. Therefore, the WCB frequencies in the analysis decrease with lead time in spring, as the WCB activity is weaker in summer than in winter, and vice versa in autumn. In winter and spring, the trajectory counts of the forecasts evolve similarly to the analysis, when considering the mean difference from the operational analysis in Figure 9a. The evolution of the trajectory count in autumn is contrary: while the WCB frequency increases in the analysis (due to the seasonal cycle), it decreases in the forecasts, leading to a large deviation at late lead times. The different seasonal behaviour is

FIGURE 9 Number of trajectories starting in the North Atlantic from operational ECMWF ensemble forecast over the years 2019 and 2020. (a) The median values (solid line) and the interquartile range (box) over 50 ensemble members, all lead times, and forecasts initialised in winter (blue), spring (green), summer (red), and autumn (yellow) averaged over both years. The darkest boxes represent the perturbed forecasts (i.e., initial condition and model physics perturbations), the pale boxes the unperturbed control forecasts, and the unfilled boxes the operational analysis. (b) Equivalent to (a), but showing the evolution of the trajectory counts with lead time. Dotted lines show the median of the perturbed ensemble members, dashed lines show the median of the unperturbed control member, and solid lines represent the median of the operational high-resolution analysis. Forecasts are classified into seasons by the initialisation date. The percentage changes described in the text always refer to the median values of the data sets [Colour figure can be viewed at wileyonlinelibrary.com]

related to the latent heating rates of the trajectories, which are larger in autumn (and summer) than in winter and spring. The offset between the perturbed (dotted lines) and unperturbed (dashed lines) forecasts is constant with lead time for the most part, similar to the results presented in Section 3.1. Note that the evolution of the trajectory counts is noisier in the unperturbed than in the perturbed case, as the time series of the former are computed with one member only.

The results presented in this section are consistent with the results obtained from the sensitivity experiments. The offset between REF and no-SPPT, with initialisations in late summer and early autumn, amounts to about 30% in the North Atlantic region (see Figure 3). This is higher than the offset in the operational data in autumn, but the qualitative signal is similar, and quantitative discrepancies might arise from interannual variability and from different time periods. Also, the sensitivity to the latent heating rate is consistent between the operational data set and the experiments: in the experiments, the role of the latent heating rate was demonstrated indirectly by analyzing different starting regions of the trajectories (e.g., larger differences between REF and no-SPPT in the Tropics than in the Extratropics) and directly by classifying the trajectories

into two heating regimes. In the operational data set, the seasonal variations of the frequency differences between perturbed and unperturbed forecasts support the hypothesis that the magnitude of the latent heating controls the effect of SPPT on the trajectories, even though it cannot be shown directly, as the latent heating rates are not available. Further, the deviations from the verifying analyses are also in accordance, with a larger underestimation of the trajectory frequencies for large heating rates (in the experiments) and in the warm season (operational data set), respectively. Finally, the consistent results across the two data sets reveal that the effect of SPPT on rapidly ascending air streams is not sensitive to the configuration of the ensemble, for example the model resolution or ensemble size, and on the details of the detection of the ascending air streams (see Table 1).

4 | DISCUSSION

In this study, we investigated the effect of the SPPT scheme on rapidly ascending air streams (i.e., extratropical WCBs and tropical convection) that are detected by trajectory analysis. By conducting sensitivity experiments

with different configurations of ECMWF's ensemble prediction system, we found that the frequency of rapidly ascending air streams is systematically increased when SPPT is activated. Even though SPPT introduces symmetric zero-mean perturbations into the forecast (Leutbecher *et al.*, 2017), the effect on rapidly ascending air streams is unidirectional: SPPT leads to more trajectories being pushed beyond the selection threshold of 600 hPa ascent within 48 hr than trajectories being restrained below the threshold. This is in accordance with, for example, the results of Tompkins and Berner (2008), who found that positive humidity perturbations are more likely to trigger convection than negative perturbations to suppress it. Similar results are reported in Vidale *et al.* (2021), where climate simulations with stochastic physics perturbations are shown to lead to a systematic increase of tropical cyclone frequencies compared with simulations without model uncertainty representations. Despite the different methodical approaches—tropical cyclone tracking in Vidale *et al.* (2021) and trajectory analysis in this study—the increase in tropical cyclone frequency is consistent with an increase in the frequency of rapidly ascending air streams in the Tropics in simulations with SPPT.

A possible process chain of how the symmetric SPPT perturbations can lead to an asymmetric response is illustrated schematically in Figure 10. It shows a highly simplified, hypothetical probability distribution of a quantity x (e.g., temperature) in a nonlinear system, which is characterized by a critical value (x_{crit}), above which the system is unstable. The phase space below the threshold x_{crit} (to the left of x_{crit}) is more densely populated than the phase space directly above the threshold (to the right of x_{crit}), where
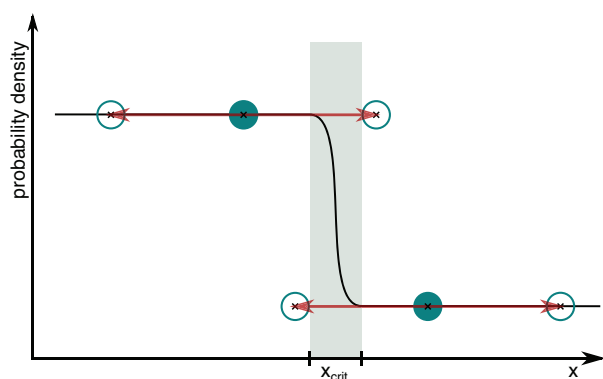
FIGURE 10 Schematic illustrating the asymmetric effect of zero-mean perturbations on variables in a nonlinear system. The black line is the probability density; the black crosses surrounded by filled circles illustrate values that are perturbed symmetrically with an amplitude given by the red arrows. The black crosses with unfilled circles show the values after the perturbation has been applied. The grey area separates stable from unstable phase space [Colour figure can be viewed at wileyonlinelibrary.com]

instabilities are instantly removed. When finite-amplitude perturbations are introduced into this system, there will be more instances of values below the threshold being pushed above the critical value by positive perturbations than values above the threshold being pushed below the critical value, as the distribution around the threshold is not uniform. Applying this concept to rapidly ascending air streams, the quantity could stand for temperature and the critical value the temperature above which convection is triggered. Thus, symmetric perturbations result in a unidirectional effect on rapidly ascending air streams. This illustrates how symmetric perturbations can result in an asymmetric response when applied in nonlinear systems.

This implies that perturbations of the initial conditions could also have a similar effect to SPPT. The reason why this is not apparent in the diagnostics presented here is that IC perturbations are only applied at the beginning of the forecast. The evolution of the trajectory count (Figure 4) as well as the omega frequency distributions (Figure 7) do not show a corresponding signal, because these are both time-integrated metrics, which hide the short-lived effect of the IC perturbations. However, considering only the first few forecast hours, we found that IC perturbations also modify fast upward velocities (not shown).

The proposed mechanism matches the hypothesis that SPPT mainly impacts the most rapid ascents in a direct manner, while changes to the slower upward and downward motions are an effect of mass balancing (see Section 3.2). Processes involved in rapid ascents are more often highly nonlinear (e.g., convective initiation) than descending motions, which favours a unidirectional response to symmetric perturbations. Therefore, it is less likely that perturbations through SPPT affect the downward motions directly. A similar argument can be used to understand the reduced occurrence of moderate upward velocities through SPPT. However, we think that the complex effect of SPPT on the whole spectrum of vertical velocities cannot be fully understood without further, more detailed experimentation—for example, tailored sensitivity experiments, which is beyond the scope of this study.

The impact of SPPT on the vertical velocities is also reflected in frequency changes of precipitation (see Section 3.3), which is in line with Subramanian *et al.* (2017), who found qualitatively similar signals. Quantitative differences between the studies most likely arise from several aspects, such as a different model version of the IFS (including changes in the SPPT scheme) and a different investigation period. Our results show that the modification of precipitation is directly linked to the altered vertical velocities, and highlights how surface weather is affected by stochastic physics perturbations.

The increased frequency of rapidly ascending air streams due to SPPT is observed for most parts of the

globe (in the sensitivity experiments) and year-round (in the operational data set), but is stronger when the latent heating of the trajectories is large (i.e., stronger in the (sub-)Tropics than in the Extratropics and stronger in the transition seasons than in winter). SPPT introduces perturbations with an amplitude proportional to the net local parametrisation tendency. If the magnitude of the perturbation is large, it is more likely that an air parcel distant from the critical value will be shifted across the threshold, than when the perturbation is small, assuming an identical base state. Therefore, the increased frequency of WCBs and tropical convection is more pronounced where the latent heating (which is proportional to the perturbation amplitude) is large. The impact of SPPT on the trajectory characteristics, such as the latent heating rate itself, is, however, very small. This goes along with the aforementioned process chain of how perturbations influence rapid ascents: air parcels are not triggered to rise because the environmental conditions have been changed by SPPT, as this would result in changed trajectory characteristics—for example, moisture accumulation in the inflow region would lead to higher heating rates. In fact, the vertical velocities are simply altered systematically as a consequence of the perturbations in the nonlinear system.

5 | CONCLUSIONS AND OUTLOOK

This study investigates the effect of the SPPT scheme on rapidly ascending air streams by computing trajectories in sensitivity experiments with ECMWF's ensemble prediction system. We showed that SPPT increases the frequency of trajectories associated with tropical convection and WCBs, and demonstrated that this behaviour is proportional to the latent heating rate along the trajectories. This systematic effect of SPPT makes rapidly ascending air streams more consistent with the verifying analysis when the latent heating rate along the trajectories is large, but reduces consistency with the analysis for small heating rates. Because of the crucial role of the latent heating rate along the trajectories, the effect of SPPT varies regionally and during the course of the year. The robustness of the results was corroborated by analyzing trajectories from operational ensemble forecasts, in which the unperturbed control member behaves identically to the experiments without SPPT. Further, an Eulerian framework illustrates that not only are fast upward velocities changed by SPPT, but all scales of vertical motion are affected. The modifications of the upward vertical velocities result in corresponding changes of the precipitation-rate frequencies. Finally, we hypothesized that the asymmetric response of rapidly ascending air streams to symmetric, zero-mean perturbations arises from nonlinearities in the initiation of

rapid ascents, and that other kinds of perturbation techniques could also result in similar effects.

It is well established that stochastic physics perturbation schemes not only have a positive impact on the ensemble reliability but also improve probabilistic forecast skill and can reduce biases (e.g., Leutbecher et al., 2017). Several studies also report a positive impact of stochastic physics on the representation of large-scale circulation regimes (e.g., Weisheimer et al., 2014; Dawson and Palmer, 2015), which is obtained from noise-induced regime transitions (Berner et al., 2015). However, none of the studies breaks down a process chain that describes the propagation of the perturbations introduced by stochastic physics to the large scale. In the Extratropics, WCBs have been shown to be an important process for the upscale propagation of errors (Baumgart et al., 2019) and for the formation and maintenance of atmospheric blocks (Pfahl et al., 2015; Steinfeld and Pfahl, 2019), which are essential features of large-scale circulation regimes. Our study provides a process-oriented perspective on stochastic physics and demonstrates that SPPT systematically changes the frequency of diabatically driven, rapidly ascending air streams, such as WCBs. Future work will try to close the process chain by assessing how the SPPT-induced effect on WCBs is propagated upscale and investigating whether changes of the large-scale circulation can be attributed to the increased frequency of WCBs.

SPPT is only one among a number of other model uncertainty schemes and it assumes that uncertainty is proportional to the net physics tendencies (Leutbecher et al., 2017). The stochastically perturbed parametrisations (SPP) scheme introduces stochastic perturbations into the physical parametrisations directly, with the aim of preserving local conservation properties (Ollinaho et al., 2017; Lang et al., 2021). Similar experiments with model uncertainty representations through SPP could provide a skill assessment regarding complex, multiscale processes, which goes beyond the classical verification scores of large-scale variables. Sensitivity experiments with different configurations of SPP—such as perturbations that are only introduced into specific parametrisation schemes—could further enhance our understanding of how stochastic perturbations interact with nonlinear processes. Finally, it would also be interesting to analyse model uncertainty schemes that introduce perturbations into components of the forecast model other than the physical parametrisations—for example, into the dynamical core.

AUTHOR CONTRIBUTIONS

Moritz Pickl: conceptualization; data curation; formal analysis; investigation; methodology; visualization; writing – original draft; writing – review and editing. **Simon T. K. Lang:** conceptualization; methodology; resources; supervision; writing – review and editing. **Martin Leutbecher:** conceptualization; resources; writing – review and editing. **Christian M. Grams:** conceptualization; funding acquisition; methodology; project administration; supervision; writing – review and editing.

ORCID

Moritz Pickl https://orcid.org/0000-0003-3853-4131
Simon T. K. Lang https://orcid.org/0000-0003-3952-586X
Martin Leutbecher https://orcid.org/0000-0003-4160-0750
Christian M. Grams https://orcid.org/0000-0003-3466-9389

REFERENCES

Baumgart, M., Ghinassi, P., Wirth, V., Selz, T., Craig, G.C. and Riemer, M. (2019) Quantitative view on the processes governing the upscale error growth up to the planetary scale using a stochastic convection scheme. *Monthly Weather Review*, 147, 1713–1731.

Berman, J.D. and Torn, R.D. (2019) The impact of initial condition and warm conveyor belt forecast uncertainty on variability in the downstream waveguide in an ECMWF case study. *Monthly Weather Review*, 147, 4071–4089.

Berner, J., Achatz, U., Batté, L., Bengtsson, L., De La Cámara, A., Christensen, H.M., Colangeli, M., Coleman, D.R., Crommelin, D., Dolaptchiev, S.I., Franzke, C.L., Friederichs, P., Imkeller, P., Järvinen, H., Juricke, S., Kitsios, V., Lott, F., Lucarini, V., Mahajajaajan, S., Palmer, T.N., Penland, C., Sakradzijaja, M., Von Storch, J.S., Weisheimer, A., Weniger, M., Williams, P.D. and Yano, J.I. (2017) Stochastic parameterization toward a new view of weather and climate models. *Bulletin of the American Meteorological Society*, 98, 565–587.

Berner, J., Fossell, K.R., Ha, S.Y., Hacker, J.P. and Snyder, C. (2015) Increasing the skill of probabilistic forecasts: understanding performance improvements from model-error representations. *Monthly Weather Review*, 143, 1295–1320.

Buizza, R., Leutbecher, M. and Isaksen, L. (2008) Potential use of an ensemble of analyses in the ECMWF Ensemble Prediction System. *Quarterly Journal of the Royal Meteorological Society*, 134, 2051–2066.

Buizza, R., Miller, M. and Palmer, T.N. (1999) Stochastic representation of model uncertainties in the ECMWF Ensemble Prediction System. *Quarterly Journal of the Royal Meteorological Society*, 125, 2887–2908.

Carlson, T.N. (1980) Airflow through midlatitude cyclones and the comma cloud pattern. *Monthly Weather Review*, 108, 1498–1509.

Christensen, H.M., Moroz, I.M. and Palmer, T.N. (2015) Simulating weather regimes: impact of stochastic and perturbed parameter schemes in a simple atmospheric model. *Climate Dynamics*, 44, 2195–2214.

Davini, P., Weisheimer, A., Balmaseda, M., Johnson, S.J., Molteni, F., Roberts, C.D., Senan, R. and Stockdale, T.N. (2021) The representation of winter Northern Hemisphere atmospheric blocking in ECMWF seasonal prediction systems. *Quarterly Journal of the Royal Meteorological Society*, 147, 1344–1363.

Dawson, A. and Palmer, T.N. (2015) Simulating weather regimes: impact of model resolution and stochastic parameterization. *Climate Dynamics*, 44, 2177–2193.

ECMWF (2019) *IFS documentation CY46R1—Part VI: Technical and computational procedures*. Reading, UK: ECMWF. URL: https://www.ecmwf.int/node/19310.

Grams, C.M. and Archambault, H.M. (2016) The key role of diabatic outflow in amplifying the midlatitude flow: a representative case study of weather systems surrounding western North Pacific extratropical transition. *Monthly Weather Review*, 144, 3847–3869.

Grams, C.M., Magnusson, L. and Madonna, E. (2018) An atmospheric dynamics perspective on the amplification and propagation of forecast error in numerical weather prediction models: a case study. *Quarterly Journal of the Royal Meteorological Society*, 144, 2577–2591.

Grams, C.M., Wernli, H., Böttcher, M., Čampa, J., Corsmeier, U., Jones, S.C., Keller, J.H., Lenz, C.J. and Wiegand, L. (2011) The key role of diabatic processes in modifying the upper-tropospheric wave guide: a North Atlantic case-study. *Quarterly Journal of the Royal Meteorological Society*, 137, 2174–2193.

Gray, S.L., Dunning, C.M., Methven, J., Masato, G. and Chagnon, J.M. (2014) Systematic model forecast error in Rossby-wave structure. *Geophysical Research Letters*, 41, 2979–2987.

Haiden, T. (2019). *Evaluation of ECMWF forecasts, including the 2019 upgrade, ECMWF Technical Memorandum 853*. Reading, UK: ECMWF. https://www.ecmwf.int/node/19277.

Hersbach, H., Bell, B., Berrisford, P., Hirahara, S., Horányi, A., Muñoz-Sabater, J., Nicolas, J., Peubey, C., Radu, R., Schepers, D., Simmons, A., Soci, C., Abdalla, S., Abellan, X., Balsamo, G., Bechtold, P., Biavati, G., Bidlot, J., Bonavita, M., De Chiara, G., Dahlgren, P., Dee, D., Diamantakis, M., Dragani, R., Flemming, J., Forbes, R., Fuentes, M., Geer, A., Haimberger, L., Healy, S., Hogan, R.J., Hólm, E., Janisková, M., Keeley, S., Laloyaux, P., Lopez, P., Lupu, C., Radnoti, G., de Rosnay, P., Rozum, I., Vamborg, F., Villaume, S. and Thépaut, J.N. (2020) The ERA5 global reanalysis. *Quarterly Journal of the Royal Meteorological Society*, 146, 1999–2049.

Jiang, H. and Zipser, E.J. (2010) Contribution of tropical cyclones to the global precipitation from eight seasons of TRMM data:

regional, seasonal, and interannual variations. *Journal of Climate*, 23, 1526–1543.

Joos, H. and Forbes, R.M. (2016) Impact of different IFS microphysics on a warm conveyor belt and the downstream flow evolution. *Quarterly Journal of the Royal Meteorological Society*, 142, 2727–2739.

Joos, H. and Wernli, H. (2012) Influence of microphysical processes on the potential vorticity development in a warm conveyor belt: a case-study with the limited-area model COSMO. *Quarterly Journal of the Royal Meteorological Society*, 138, 407–418.

Lang, S.T., Lock, S.J., Leutbecher, M., Bechtold, P. and Forbes, R.M. (2021) Revision of the Stochastically Perturbed Parametrisations model uncertainty scheme in the Integrated Forecasting System. *Quarterly Journal of the Royal Meteorological Society*, 147, 1364–1381.

Leutbecher, M., Lock, S.J., Ollinaho, P., Lang, S.T., Balsamo, G., Bechtold, P., Bonavita, M., Christensen, H.M., Diamantakis, M., Dutra, E., English, S., Fisher, M., Forbes, R.M., Goddard, J., Haiden, T., Hogan, R.J., Juricke, S., Lawrence, H., MacLeod, D., Magnusson, L., Malardel, S., Massart, S., Sandu, I., Smolarkiewicz, P.K., Subramanian, A., Vitart, F., Wedi, N. and Weisheimer, A. (2017) Stochastic representations of model uncertainties at ECMWF: state of the art and future vision. *Quarterly Journal of the Royal Meteorological Society*, 143, 2315–2339.

Leutbecher, M. and Palmer, T.N. (2008) Ensemble forecasting. *Journal of Computational Physics*, 227, 3515–3539.

Lock, S.J., Lang, S.T., Leutbecher, M., Hogan, R.J. and Vitart, F. (2019) Treatment of model uncertainty from radiation by the Stochastically Perturbed Parametrization Tendencies (SPPT) scheme and associated revisions in the ECMWF ensembles. *Quarterly Journal of the Royal Meteorological Society*, 145, 75–89.

Lorenz, E. (1963) Deterministic Nonperiodic Flow. *Journal of the Atmospheric Sciences*, 20, 130–141.

Maddison, J.W., Gray, S.L., Martínez-Alvarado, O. and Williams, K.D. (2020) Impact of model upgrades on diabatic processes in extratropical cyclones and downstream forecast evolution. *Quarterly Journal of the Royal Meteorological Society*, 146, 1322–1350.

Madonna, E., Boettcher, M., Grams, C.M., Joos, H., Martius, O. and Wernli, H. (2015) Verification of North Atlantic warm conveyor belt outflows in ECMWF forecasts. *Quarterly Journal of the Royal Meteorological Society*, 141, 1333–1344.

Madonna, E., Wernli, H., Joos, H. and Martius, O. (2014) Warm conveyor belts in the ERA-Interim Dataset (1979–2010). Part I: climatology and potential vorticity evolution. *Journal of Climate*, 27, 3–26.

Martínez-Alvarado, O., Madonna, E., Gray, S.L. and Joos, H. (2016) A route to systematic error in forecasts of Rossby waves. *Quarterly Journal of the Royal Meteorological Society*, 142, 196–210.

Mazoyer, M., Ricard, D., Rivière, G., Delanoë, J., Arbogast, P., Vié, B., Lac, C., Cazenave, Q. and Pelon, J. (2021) Microphysics impacts on the warm conveyor belt and ridge building of the NAWDEX IOP6 cyclone. *Monthly Weather Review*, 149, 3961–3980.

Ollinaho, P., Lock, S.J., Leutbecher, M., Bechtold, P., Beljaars, A., Bozzo, A., Forbes, R.M., Haiden, T., Hogan, R.J. and Sandu, I. (2017) Towards process-level representation of model uncertainties: stochastically perturbed parametrizations in the ECMWF ensemble. *Quarterly Journal of the Royal Meteorological Society*, 143, 408–422.

Pfahl, S., Madonna, E., Boettcher, M., Joos, H. and Wernli, H. (2014) Warm conveyor belts in the ERA-Interim Dataset (1979–2010).

Part II: moisture origin and relevance for precipitation. *Journal of Climate*, 27, 27–40.

Pfahl, S., Schwierz, C., Croci-Maspoli, M., Grams, C.M. and Wernli, H. (2015) Importance of latent heat release in ascending air streams for atmospheric blocking. *Nature Geoscience*, 8, 610–614.

Rabier, F., Järvinen, H., Mahfouf, J.F. and Simmons, A. (2000) The ECMWF operational implementation of four-dimensional variational assimilation. I: experimental results with simplified physics. *Quarterly Journal of the Royal Meteorological Society*, 126, 1143–1170.

Rivière, G., Wimmer, M., Arbogast, P., Piriou, J.-M., Delanoë, J., Labadie, C., Cazenave, Q. and Pelon, J. (2021) The impact of deep convection representation in a global atmospheric model on the warm conveyor belt and jet stream during NAWDEX IOP6. *Weather and Climate Dynamics*, 2, 1011–1031.

Rodwell, M.J., Magnusson, L., Bauer, P., Bechtold, P., Bonavita, M., Cardinali, C., Diamantakis, M., Earnshaw, P., Garcia-Mendez, A., Isaksen, L., Källén, E., Klocke, D., Lopez, P., McNally, T., Persson, A., Prates, F. and Wedi, N. (2013) Characteristics of occasional poor medium-range weather forecasts for Europe. *Bulletin of the American Meteorological Society*, 94, 1393–1405.

Rodwell, M.J., Richardson, D.S., Parsons, D.B. and Wernli, H. (2018) Flow-dependent reliability: a path to more skillful ensemble forecasts. *Bulletin of the American Meteorological Society*, 99, 1015–1026.

Sánchez, C., Methven, J., Gray, S. and Cullen, M. (2020) Linking rapid forecast error growth to diabatic processes. *Quarterly Journal of the Royal Meteorological Society*, 146, 3548–3569.

Schäfler, A., Craig, G., Wernli, H., Arbogast, P., Doyle, J.D., Mctaggart-Cowan, R., Methven, J., Rivière, G., Ament, F., Boettcher, M., Bramberger, M., Cazenave, Q., Cotton, R., Crewell, S., Delanoë, J., Dörnbrack, A., Ehrlich, A., Ewald, F., Fix, A., Grams, C.M., Gray, S.L., Grob, H., Groß, S., Hagen, M., Harvey, B., Hirsch, L., Jacob, M., Kölling, T., Konow, H., Lemmerz, C., Lux, O., Magnusson, L., Mayer, B., Mech, M., Moore, R., Pelon, J., Quinting, J., Rahm, S., Rapp, M., Rautenhaus, M., Reitebuch, O., Reynolds, C.A., Sodemann, H., Spengler, T., Vaughan, G., Wendisch, M., Wirth, M., Witschas, B., Wolf, K. and Zinner, T. (2018) The north Atlantic waveguide and downstream impact experiment. *Bulletin of the American Meteorological Society*, 99, 1607–1637.

Sprenger, M. and Wernli, H. (2015) The LAGRANTO Lagrangian analysis tool – Version 2.0. *Geoscientific Model Development*, 8, 2569–2586.

Steinfeld, D. and Pfahl, S. (2019) The role of latent heating in atmospheric blocking dynamics: a global climatology. *Climate Dynamics*, 53, 6159–6180.

Stockdale, T., Alonso-Balmaseda, M., Johnson, S., Ferranti, L., Molteni, F., Magnusson, L., Tietsche, S., Vitart, F., Decremer, D., Weisheimer, A., Roberts, C.D., Balsamo, G., Keeley, S., Mogensen, K., Zuo, H., Mayer, M. and Monge-Sanz, B.M. (2018) *SEAS5 and the future evolution of the long-range forecast system.* ECMWF Technical Memorandum 835. Reading, UK: ECMWF. URL: https://www.ecmwf.int/node/18750.

Subramanian, A., Weisheimer, A., Palmer, T., Vitart, F. and Bechtold, P. (2017) Impact of stochastic physics on tropical precipitation in the coupled ECMWF model. *Quarterly Journal of the Royal Meteorological Society*, 143, 852–865.

Teubler, F. and Riemer, M. (2016) Dynamics of Rossby wave packets in a quantitative potential vorticity-potential temperature framework. *Journal of the Atmospheric Sciences*, 73, 1063–1081.

Tompkins, A.M. and Berner, J. (2008) A stochastic convective approach to account for model uncertainty due to unresolved humidity variability. *Journal of Geophysical Research Atmospheres*, 113, 1–12.

Vidale, P.L., Hodges, K., Vannière, B., Davini, P., Roberts, M.J., Strommen, K., Weisheimer, A., Plesca, E. and Corti, S. (2021) Impact of stochastic physics and model resolution on the simulation of tropical cyclones in climate GCMs. *Journal of Climate*, 34, 4315–4341.

Wang, J.W.A., Sardeshmukh, P.D., Compo, G.P., Whitaker, J.S., Slivinski, L.C., McColl, C.M. and Pegion, P.J. (2019) Sensitivities of the NCEP global forecast system. *Monthly Weather Review*, 147, 1237–1256.

Weisheimer, A., Corti, S., Palmer, T. and Vitart, F. (2014) Addressing model error through atmospheric stochastic physical parametrizations: impact on the coupled ECMWF seasonal fore-casting system. *Philosophical Transactions of the Royal Society A: Mathematical, Physical and Engineering Sciences*, 372, 20130290.

Wernli, H. and Davies, H.C. (1997) A Lagrangian-based analysis of extratropical cyclones. I: the method and some applications. *Quarterly Journal of the Royal Meteorological Society*, 123, 467–489.

Zhang, F., Bei, N., Rotunno, R., Snyder, C. and Epifanio, C.C. (2007) Mesoscale predictability of moist baroclinic waves: convection-permitting experiments and multistage error growth dynamics. *Journal of the Atmospheric Sciences*, 64, 3579–3594.